Do the bridging angle affect the luminescent properties of $[(CO)_3(phen)Re(\mu\text{-}OH)Re(phen)(CO)_3]^+$?. An experimental and computational study on three polymorphs

Carolina Muñoz,[a] Marianela Saldías,[a,b] Poldie Oyarzún,[c] Jean-Yves Saillard,[d] Jean-René Hamon,[d] Guillaume Calvez,[e] Nancy Pizarro,[a] Andrés Vega[a,f]*

[a] *Universidad Andres Bello, Facultad de Ciencias Exactas, Departamento de Ciencias Químicas,* Av. Quillota 980, *Viña del Mar, Chile.*
[b] *Instituto de investigación en Innovación en Salud, Facultad de Ciencias de la Salud, Universidad Central, Lord Cochrane 417, Santiago, Chile.*
[c] *Laboratorio de Análisis de Sólidos, Departamento de Ciencias Químicas, Universidad Andrés Bello, Chile.*
[d] *Univ Rennes, CNRS, ISCR - UMR 6226, F-35000 Rennes, France.*
[e] *Univ Rennes, INSA Rennes, CNRS, ISCR - UMR 6226, F-35000 Rennes, France.*
[f] *Centro para el Desarrollo de la Nanociencia y la Nanotecnología, CEDENNA.*

The authors dedicate this work with best wishes to their distinguished colleague and friend Prof. David Carrillo at the occasion of his 80th birthday.

* *Corresponding author.* e-mail address: andresvega@unab.cl (A. Vega)

Abstract. The reaction of $[Re^{I}Br(CO)_3(THF)]_2$ with phenanthroline in solution leads to the diimine rhenium(I)tricarbonyl $[(phen)Re(CO)_3Br]$ and the dimer $[(CO)_3(phen)Re(\mu\text{-}OH)(phen)Re(CO)_3]^+Br^-$ (**1**$^+$Br$^-$) as a by-product (~ 5% yield). This latter bimetallic compound crystallizes as a mixture of three polymorphs, with variable amount of solvent: **1**$^+$Br$^-\cdot CHCl_3$ (triclinic and orthorhombic) and **1**$^+$Br$^-\cdot 2(CHCl_3)$ (triclinic). Rietveld analysis showed 38, 54 and 8% of **1**$^+$Br$^-\cdot CHCl_3$ (triclinic), **1**$^+$Br$^-\cdot CHCl_3$ (orthorhombic) and **1**$^+$Br$^-\cdot 2(CHCl_3)$ (triclinic) respectively. The **1**$^+$ cation shows two $[Re^{I}(phen)(CO)_3]^+$ units connected by means of a central hydroxyl group. Noteworthy, the bridging Re–O–Re angle varies between 130.9(7)° to 140.7(2)° along the polymorphic series. UV-vis spectrum for the **1**$^+$ shows a broad absorption band around 390 nm in CH_2Cl_2 which has been attributed to has MLCT character ($Re(d_\pi)\rightarrow\pi^*(phen)$) as confirmed by DFT. Excitation at 405 nm in solution leads to emission at 595 nm (DCM), 605 nm (DMF) and 625 nm (CH_3CN). The emission follows a mono-exponential law of decay and has lifetime of 405.8 ns (DCM). The solid-state polymorphic mixture absorbs around 460 nm. Excitation of the solid at 320 nm leads to emission with a maximum at 575 nm, which follow a bi-exponential law of decay with two components, a short one τ_1 of 27.0 ns and longer one τ_2 of 178.5 ns. These results suggest that the emitting state does not vary as function of the molecular geometry.

Keywords: Rhenium; Luminescence; Density functional calculations; polymorphism; bridging angle.

1. Introduction

Rhenium(I) tricarbonyl complexes with diimines have attracted the attention of researchers during the last decades because of their useful photophysical properties, well-behaved and predictable synthesis, stability and potential applications [1-3]. Potential applications ranges from photosensitization [4-8], anion sensing [9, 10], biolabeling and therapy [11-15], to carbon dioxide photoreduction [5, 16-23]. They typically exhibit light absorption in the UV-Vis region, mainly from metal to ligand charge transfer (MLCT) transitions [24-26].

These compounds are frequently prepared cleanly and in good yields by the reaction of a rhenium(I) carbonyl precursor and the chelating diimine with the required stoichiometry, although we showed recently that the use of a distinct stoichiometric ratio led to the formation of dimers like $[(CO)_3(phen)Re(\mu\text{-}Br)Re(phen)(CO)_3]^+[(CO)_3Re(\mu\text{-}Br)_3Re(CO)_3]^-$ (Scheme 1, right) [27].

We suspect that dimers of the type $[(CO)_3(N,N\text{-}diimine)Re(\mu\text{-}X)Re(N,N\text{-}diiimine)(CO)_3]^+$ may be a general minor by-products of the synthesis of monometallic rhenium(I) tricarbonyls. This is probably the reason why there are just limited reports on their structure [27-31]. All of them have a hydroxyl group between the rhenium centers and 2,2'-bipyridine as diimine. Moreover, to the best of our knowledge, only a single report has been published on their spectroscopic properties [27].

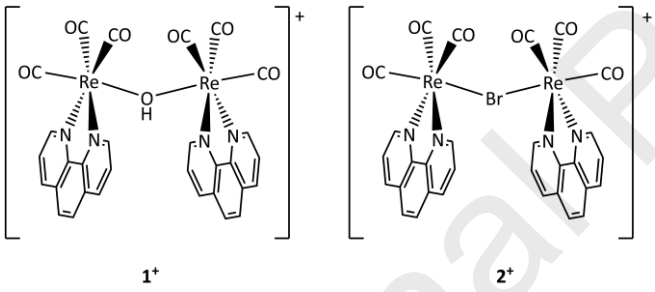

Scheme 1. Schematic structures of the cations $[(CO)_3(phen)Re(\mu\text{-}OH)(phen)Re(CO)_3]^+$ (**1**$^+$) and $[(CO)_3$ $(phen)Re(\mu\text{-}Br)(phen)Re(CO)_3]^+$ (**2**$^+$) [27]**.**

In the present article, we describe the isolation of $[(CO)_3(phen)Re(\mu\text{-}OH)Re(phen)(CO)_3]^+Br^-$ (**1**$^+$Br$^-$), as three polymorphic forms, from the reaction of $[Re^IBr(CO)_3(THF)]_2$ and 1,10-phenanthroline monohydrate. We discuss the structural and spectroscopic properties of the μ-OH bridged dimer **1**$^+$Br$^-$ and compare them with those of $[(CO)_3(phen)Re(\mu\text{-}Br)Re(phen)(CO)_3]^+[(CO)_3Re(\mu\text{-}Br)_3Re(CO)_3]^-$ (**2**$^+$$[(CO)_3Re(\mu\text{-}Br)_3Re(CO)_3]^-$), which has a bigger and better π-donating anion connecting the metal centers compared to **1**$^+$Br$^-$, which would impose some important differences both structurally and spectroscopically. We also analyze the effect of the bridging angle between the two rhenium(I) centers over its spectroscopic properties.

2. Experimental

2.1 Materials and Methods: All reagents, $(Re(CO)_3(OC_4H_8)Br)_2$, 1,10- phenanthroline monohydrate were used as provided from supplier (Aldrich), with no purification before use. Dichloromethane (DCM), acetonitrile (MeCN), ethanol (EtOH), dimethylformamide (DMF) of spectroscopic grade, Uvasol® Merck, and chloroform ($CHCl_3$) Seccosolv®Merck, were employed as received. Infrared spectra in the 4000–400 cm^{-1} region was recorded from KBr pellets on a Shimadzu Prestige 21 labstation FTIR. ^1H and ^{13}C NMR spectra were recorded on a Bruker Avance III 400 Instrument. All NMR spectra are reported in parts per million (ppm, δ) relative to tetramethylsilane (Me_4Si), with the residual solvent proton and carbon resonances used as internal standards. Elemental analysis was conducted on a Thermo-Finnigan Flash EA 1112 CHNS/O analyzer by the Microanalytical Service of the Centre Régional de Mesures Physiques de l'Ouest (CRMPO, Université de Rennes 1, France).

2.2 Synthesis of 1$^+$Br$^-$. A 100 mL flask was loaded with a magnetic stir bar, $[Re^IBr(CO)_3(THF)]_2$ (0.592 mmol, 500.0 mg), and 10 mL of chloroform, forming a pale yellow solution. After 5 min of stirring, a colorless solution of 1,10-phenanthroline monohydrate (1.184 mmol, 215.5 mg) in 30 mL of chloroform was added dropwise. A precipitate formed immediately, and the stirring was continued for an additional time of 10 min at room temperature. The solid residue was filtered, washed two times with chloroform (3 mL portion), isolated as a yellow microcrystalline solid (481.6

mg, 95 % yield), and identified as the mononuclear $[(CO)_3(phen)ReBr]$ complex by comparison of its spectroscopic parameters with those of an authentic sample.[28] The orange filtrate was evaporated to dryness under reduced pressure, affording 26.8 mg (4.8 % yield) of $\mathbf{1}^{+}Br^{-}$, isolated as a yellow-orange powder. IR (KBr): $\bar{\upsilon}$ = 2016(s), 1923(s), 1893(s) (CO) cm^{-1}. ^{1}H NMR (400 MHz, CD_2Cl_2, 298 K): δ = 7.32 (s, $CHCl_3$), 7.82 (dd, $^{3}J_{HH}$ = 4.0 Hz, H_{β} phen), 7.9 (dd, $^{3}J_{HH}$ = 4.0 Hz, $H_{\beta'}$ phen'), 8.04 (s, H_{β} phen), 8.08 (s, $H_{\delta'}$ phen'), 8.59 (dd, $^{3}J_{HH}$ = 8.0 Hz, H_{γ} phen), 8.61 (dd, $^{3}J_{HH}$ = 8.0 Hz, $H_{\gamma'}$ phen'), 9.28 (d, $^{3}J_{HH}$ = 8.0 Hz, H_{α} phen), 9.40 (d, $^{3}J_{HH}$ = 8.0 Hz, $H_{\alpha'}$ phen') ppm. $^{13}C\{^{1}H\}$ NMR (100 MHz, CD_2Cl_2, 298 K): δ = 78.11 (s, $CHCl_3$), 126.28 (CH_{β}, phen), 126.38 ($C'H_{\beta}$, phen'), 128.08 (CH_{δ}, phen), 128.22 ($C'H_{\delta}$, phen'), 131.42 (C_{quat}, phen), 138.78 (CH_{γ}, phen), 139.42 ($C'H_{\gamma}$, phen), 147.68 (C_{quat}, phen), 153.67 (CH_{α}, phen), 154.47 ($C'H_{\alpha}$, phen') ppm. Anal. Calc. for $C_{30}H_{17}N_4O_7BrRe_2 \cdot 0.55CHCl_3$: C, 34.47; H, 1.65; N, 5.26. Found: C, 34.13; H, 1.71; N, 5.02%.

2.3 Structural Determination: Single crystals of $\mathbf{1}^{+}Br^{-}$ suitable for X-ray diffraction analysis were obtained by slow evaporation of a saturated chloroform solution. Three types of differently shaped crystals formed. They were separated by hand under a microscope, and one well-shaped crystal of each type was selected for X-ray structure determination. The crystal structure of the three compounds at room temperature was determined by X-ray diffraction. Data collection were done on a SMART CCD diffractometer using ω–scans as collection strategy. Data sets were reduced using SAINT [32], while the structures were solved by direct methods and then completed by difference Fourier synthesis. Refinement by least-squares were done by using SHELXL [33, 34]. Empirical absorption corrections were applied using SADABS [32]. The hydrogen atom positions were calculated after each cycle of refinement with SHELXL using a riding model for each structure, with C—H distance of 0.93 or 0.98 Å and U_{iso}(H) of 1.2 times the parent atom, except the hydroxyl-hydrogen atom. For $\mathbf{1}^{+}Br^{-}\cdot CHCl_3$ (triclinic) it was located into the Fourier difference map and then refined with the restrain that the oxygen to hydrogen distance must be equal to 0.85 Å. Efforts to locate the hydroxyl hydrogen atoms on the other two polymorphs were unsuccessful. Their positions were calculated based on geometric arguments and then refined with restrictions. Table S1 shows crystallographic and refinement details for each of the three polymorphs.

2.4 Powder Diffraction and Rietveld analysis. The mixture of polymorphs $\mathbf{1}^{+}Br^{-}\cdot CHCl_3$ (triclinic), $\mathbf{1}^{+}Br^{-}\cdot CHCl_3$ (orthorhombic), $\mathbf{1}^{+}Br^{-}\cdot 2(CHCl_3)$ (triclinic) was mounted on a zero-background cell. The X-ray powder pattern was measured on a Bruker D8 Advance diffractometer (40 kV, 30 mA, 5°–70° 2θ in 0.020 2144° steps, 0.5 s $step^{-1}$) equipped with a LynxEye position sensitive detector. The lower window of the detector electronics was increased using Si-Einkristalle as sample port from its default value of 0.11–0.19 V to minimize the effects of fluorescence. The Rietveld refinement [35] as implemented into the Diffrac. TOPAS suite version 4.2 [36] was used to determine the quantitative composition of the solid. The single crystal structure information of $\mathbf{1}^{+}Br^{-}\cdot CHCl_3$ (triclinic), $\mathbf{1}^{+}Br^{-}\cdot CHCl_3$ (orthorhombic), $\mathbf{1}^{+}Br^{-}\cdot 2(CHCl_3)$ (triclinic) has been used as determined in this work. Using this technique, the reported peak positions were derived from the extracted integrated intensities, and positions calculated from the lattice parameters. The quantitative phase analysis is obtained from the scale factor, which is calculated using the number of molecules per unit cell, the molecular mass, and the unit cell volume and absorption contrast factor.

2.5 Solution spectroscopic and photophysical measurements. UV-Vis spectra were recorded on an Agilent 8453 Diode-Array spectrophotometer in the range of 250-700 nm in aerated solvent

solutions at room temperature. Emission spectra were measured in a Horiba Jobin-Yvon FluoroMax-4 spectrofluorometer in different solvents at room temperature. Luminescence lifetime measurements were carried out with the time correlated single photon counting technique using a PicoQuant FluoTime300 fluorescence lifetime spectrometer. A sub-nanosecond Pulsed Laser 405 nm was employed as pulsed light sources (FWHM ~ 500 ps; average power 2 mW). Time resolved experiments were made in solution either air-equilibrated or argon-saturated. Emission quantum yields (Φ_{em}) were measured using the procedures described in the literature with $[Ru(bpy)_3](Cl)_2$ in acetonitrile solution as the actinometer [37, 38]. Singlet oxygen, $O_2(^1\Delta_g)$, emission measurements were carried out with the FluoTime 300 spectrometer. For the detection at 1270 nm, a NIR PMT H10330A (Hamamatsu) was employed. The $O_2(^1\Delta_g)$ quantum yields (Φ_Δ) were determined by comparing the intensity at zero time of the 1270 nm signals to those of optically-matched solutions of perinaphthenone (PNF) or $[Ru(bpy)_3](Cl)_2$ as references [39, 40].

2.6 Solid-state spectroscopy and photophysical measurements. The UV/VIS absorption spectrum was recorded with a Perkin Elmer Lambda 650 double beam spectrometer between 200 and 900 nm, using both a Xe and a deuterium lamp switching at 319 nm equipped with a Perkin Elmer 60 mm integrating sphere, operating in double beam mode. The slits were fixed at 2 nm and the step size at 1.4 nm for a resulting scanning speed of 300 nm per minute. The emission and excitation spectra were measured with a Horiba Jobin-Yvon Fluorolog III spectrometer, using a monochromated Xe bulb as ultraviolet source and a monochromated FL-1073 room temperature R928P emission signal detector (190-860 nm). The excitation and emission slits were both fixed at 3 nm. The excitation spectrum was recorded every 0.5 nm between 280 and 500 nm with an integration time of 200 ms and a KV500 cut-off filter (at 500 nm); the fixed emission wavelength was 580 nm; a few milligrams of sample being available, twenty spectra were accumulated for a better signal on noise reduction. The emission spectrum was recorded every nanometer between 380 and 850 nm with an integration time of 200 ms and a KV370 cut-off filter (at 370 nm); the fixed excitation wavelength was 328 nm, the highest intensity of the excitation spectrum. Ten spectra were accumulated. The emission lifetime measurement was performed with the same Horiba Jobin-Yvon Fluorolog III spectrometer, using a Horiba time-correlated single photon counting FluoroHub with a DD-320 pulsed LED source at 320 ± 10 nm (typical pulse 1 ns at 20 MHz). The emission wavelength was fixed at 580 nm, emission slit at 3 nm, the measuring window was 400 ns giving operating conditions of about 0.1 ns per channel on the 4096 channels of the FluoroHub. In order to de-correlate the decreasing of the intensity of the LED from the decreasing of the emission of the sample, we first measured the lifetime on a diffusing solution of nanometric silica, then we measured the lifetime of the sample in the same conditions in a Hellma Analytics high precision cell that is adapted for solid samples.

2.7 Computational details. All geometry optimizations were performed at the B3LYP/6-31+G(d,p) level of theory using the Gaussian09 Rev C.01 package of programs (G09) [41], and using the crystallographic coordinates as input. The LANL2DZ basis set was used only for rhenium. Empirical dispersion corrections were introduced for some optimizations by using the method of Grimme [42] as implemented in Gaussian 09. The optimized geometries were characterized as true minimum on their potential energy surface by harmonic vibrational analysis (no imaginary frequency found). Table S2 shows a comparison of the main interatomic distances with those determined by single crystal diffraction. Excited

state calculations were performed within the time-dependent density functional theory (TD-DFT) methodology as implemented in G09. Absorption spectra were simulated from the above calculations using the GaussSum 3.0 suite of freely available processing tools. A full width at half-maximum (FWHM) of the Gaussian curves corresponding to 2500 cm^{-1} was employed to convolute the spectrum. Representations of molecular orbitals were generated using the G09 cubegen tool and have been visualized using VMD and Povray 3.6 programs [43, 44].

3. Results and Discussions

3.1 Synthesis and composition of the polymorphic mixture. Complex **1**$^{+}$Br^{-} was formed as a side product of the reaction of $[Re^{I}Br(CO)_3(THF)]_2$ and 1,10-phenanthroline monohydrate in the 1:2 stoichiometric ratio, in chloroform at room temperature. It was isolated as a yellow-orange powder in 5% yield; the major product of the reaction being the known $[Re^{I}Br(CO)_3(phen)]$ [45]. The solid-state IR spectrum of **1**$^{+}$Br^{-} exhibits three intense CO vibrations at 2016, 1923 and 1893 cm^{-1} that characterizes it as a facial isomer [46]. The O-H stretching vibration cannot be observed being hidden by the very broad band of the phen ligand in the 3600-3100 cm^{-1} region. Well-resolved ^{1}H and ^{13}C NMR spectra of **1**$^{+}$Br^{-} confirm the diamagnetic ground state of Re^{I} in the bimetallic cation **1**$^{+}$. Both spectra show two close sets of resonances in an approximative 2:1 ratio, presumably due to a mixture of *fac* isomers [46]. Besides the signal of the chloroform crystallization molecule, the ^{1}H NMR spectrum exhibits two sets of four resonances attributed to the four types of phen protons, in the range δ = 7.82-9.40 ppm (see Exp. Sect. For details), in agreement with reported data for $[Re^{I}X(CO)_3(phen)]$ species [47]. The hydroxyl proton could not be observed. In the ^{13}C NMR spectrum, the six magnetically nonequivalent carbons of the phenanthroline ligand are observed for the major isomer, while the two quaternary carbons of the minor one does not show up. The fact that those latter carbons nor the carbonyl signals of both isomers could not be observed is probably due to the low solubility of **1**$^{+}$Br^{-} in CD_2Cl_2. In addition, composition and structure of the binuclear complex were authenticated by satisfactory combustion analysis and single-crystal X-ray diffraction study.

It has been previously described that adventitious water may lead to rhenium-aquo species [48]. For $[(phen)(H_2O)Re(CO)_3]^{+}(CF_3SO_3)^{-}$, the triflate anion forms hydrogen bonds with the coordinated water molecule, moreover the hydrogen bonding capacity has been argued to influence the spectroscopy of the cation [48]. For the present case one would suppose that the aquo cation reacts with other rhenium(I) species present in solution to lead to the dimeric $[(CO)_3(phen)Re(\mu\text{-}OH)Re(phen)(CO)_3]^{+}$ (**1**$^{+}$) cation. The experimental powder XRD pattern measured for the mixture of the three polymorphs is shown in Figure 1.

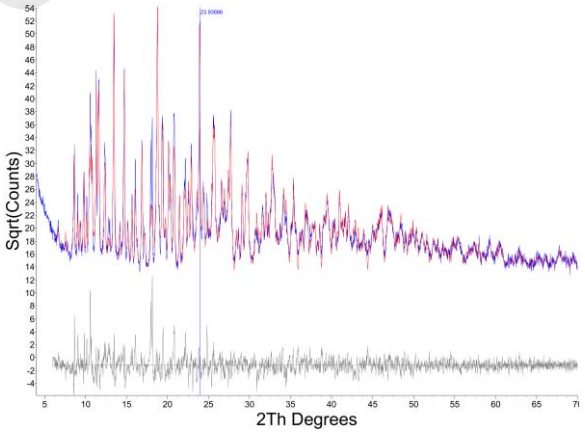

Figure 1: Rietveld refinement pattern for the polymorphic mixture of **1**$^{+}$Br^{-}: $1^{+}Br^{-}\cdot CHCl_3$ (triclinic), $\mathbf{1}^{+}Br^{-}\cdot CHCl_3$ (orthorhombic) and $\mathbf{1}^{+}Br^{-}\cdot 2(CHCl_3)$ (triclinic). The observed data are indicated by solid line (blue) and the calculated data by the solid line overlying them (red). The lower curve shows the difference between the observed and calculated powder diffraction patterns. The observed and calculated data are offset 10 Sqrt(Counts), from the lower axis.

The observed data are indicated by the blue line while the red one represents those computed by using the Rietveld analysis with the crystallographic details for the polymorphic forms of the compound: **1**$^{+}$Br^{-}·$CHCl_3$ (triclinic), **1**$^{+}$Br^{-}·$CHCl_3$ (orthorhombic) and **1**$^{+}$Br^{-}·2($CHCl_3$) (triclinic). The lower curve, drawn in black, shows the difference between the observed and calculated powder diffraction patterns. The Table S3 provides the crystallographic data for **1**$^{+}$Br-·$CHCl_3$ (Triclinic), $1^{+}Br^{-}$·$CHCl_3$ (Orthorhombic), $1^{+}Br^{-}$ ·$(CHCl_3)_2$(Triclinic) which include weight percent (wt% Rietveld) and refinement parameter results, respectively (GOF,Rs). Figure S1 shows details of the contribution of each phase to the powder pattern measured for the polymorphic mixture. It mainly states that the solid still contains some remaining [(phen)Re$(CO)_3$Br]. If this is removed, the compound **1**$^{+}$Br^{-} is obtained as a polymorphic mixture composed by a 38% of **1**$^{+}$Br^{-}·$CHCl_3$ (triclinic), 54% of **1**$^{+}$Br^{-}·$CHCl_3$ (orthorhombic) and 8 % of **1**$^{+}$Br^{-}·2($CHCl_3$) (triclinic).

3.2 Structural Description. The (**1**$^{+}$) cation is built by two cationic [Re^{I}(phen)$(CO)_3]^{+}$ units, connected by an hydroxyl anion. The geometry for each Re^{I} center is a non-regular octahedron with the carbonyls having facial geometry, and the cation could be described as to be composed of two one vertex-sharing octahedron, as shown in Figure 2.
Table 1 displays selected bond and interatomic distances for each phase. **2**$^{+}$[$(CO)_3$Re(μ-$Br)_3$Re$(CO)_3]^{-}$ has been added for comparison. The Re2—O1—Re1 angle varies from 130.9(7)° ($1^{+}Br^{-}$ ·$CHCl_3$, orthorhombic phase) to 140.70(19)° (**1**$^{+}$Br^{-} ·$CHCl_3$, triclinic phase). The angle is at least 10° larger than the value observed for **2**$^{+}$ (Re2—Br1—Re1, 119.7(3)°). This suggests that this parameter is subjected to changes by the packing structure. The shorter rhenium to oxygen distance compared to rhenium bromide and the larger value of the angle makes the Re1···Re2 distance in **1**$^{+}$ (~ 4.0 Å) shorter than the measured value in **2**$^{+}$(~ 4.6 Å).[27]

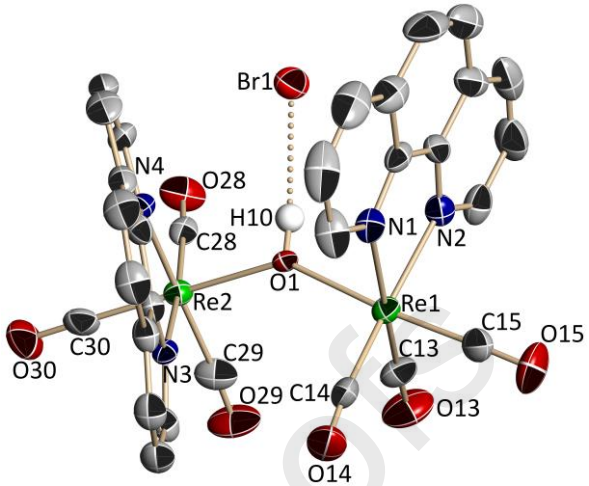

Figure 2. Molecular structure of **1**$^{+}$Br^{-} (from **1**$^{+}$Br^{-} ·$CHCl_3$, triclinic phase). Hydrogens on the phenanthroline and the molecule of solvent were omitted for clarity. Displacement ellipsoids at 50%.

Table 1. Bond and interatomic distances (Å) and angles (°) for **1**$^{+}$Br^{-}·$CHCl_3$ (triclinic), $1^{+}Br^{-}$·$CHCl_3$ (orthorhombic), **1**$^{+}$Br^{-}·2($CHCl_3$) (triclinic) and for comparison **2**$^{+}$($Re_2Br_3(CO)_6)^{-}$ [27]. The DFT-optimized distances determined for **1**$^{+}$ were included for comparison

	1^{+}Br^{-}·$CHCl_3$ (Triclinic)	**1**$^{+}$Br^{-} ·2$CHCl_3$	**1**$^{+}$Br^{-}·$CHCl_3$ (Orth.)	**2**$^{+}$ ($Re_2Br_3(CO)_6)^{-}$	**1**$^{+}$ (DFT)
Re1—C13	1.911(8)	1.853(14)	1.87(3)		1.925
Re1—C14	1.907(7)	1.889(17)	1.91(3)		1.923
Re1—C15	1.894(8)	1.878(15)	1.74(3)		1.925
Re2—C28	1.895(6)	1.904(16)	1.86(3)		1.923
Re2—C29	1.937(8)	1.882(16)	1.90(3)		1.925
Re2—C30	1.915(8)	1.894(16)	1.80(3)		1.925
Re1—N1	2.181(5)	2.150(10)	2.184(19)		2.224
Re1—N2	2.184(5)	2.199(11)	2.15(2)		2.224
Re1—O1	2.149(4)	2.158(8)	2.149(13)		2.207
Re2—N3	2.170(4)	2.177(10)	2.20(2)		2.224
Re2—N4	2.183(5)	2.164(10)	2.09(2)		2.224
Re2—O1	2.159(4)	2.144(8)	2.144(13)		2.207
Re1···Re2	4.0570(7)	3.955(2)	3.906(2)	4.5866(10)	4.177
Re2-O1-Re1	140.70(19)	133.7(4)	130.9(7)		
Re2-Br1-Re1				119.7(3)	142.3

It is important to note that both metal-phenanthroline fragments are not co-planar, but they define a dihedral angle of 41.2(2)°, 58.65(9)° and 43.3(2)° for **1**$^{+}$Br^{-}·2($CHCl_3$) (triclinic), **1**$^{+}$Br^{-} ·$CHCl_3$ (orthorhombic) and **1**$^{+}$Br^{-}·$CHCl_3$ (triclinic)

respectively. The corresponding value for **2**$^{+}$[(CO)$_3$Re(μ-Br)$_3$Re(CO)$_3$]$^{-}$ is 32.7(1)° [27]. Noteworthy, the bromide counter-anion occupy a well-defined position near to hydroxyl group allowing the definition of a rather intimate hydrogen bond, with D···A equal to 3.362(4) Å, 3.353(9) Å and 3.479(15) Å for **1**$^{+}$Br^{-}·CHCl$_3$ (triclinic), **1**$^{+}$Br^{-}·2(CHCl$_3$) (triclinic) and **1**$^{+}$Br^{-}·CHCl$_3$ (orthorhombic) respectively. Table S4 shows complete details of the hydrogen bonds and weak interactions present in each packing.

3.3 Electronic Structure. In order to have a better understanding of the electronic structure of cation 1^{+} and the spectroscopic properties, specially concerning the effect of the bridging angle, we have performed DFT modeling based on the crystal structure determined by X-rays diffraction. Although an ideal C_{2v} (or C_2 or C_s) symmetry could be anticipated for **1**$^{+}$, its fully optimized geometry was found to be of C_1 symmetry. This is the result of a twisting imposed by the carbonyls on each rhenium site.

Although no symmetry relation is found between both [(phen)Re(CO)$_3$]$^{+}$ fragments, they are very similar in electronic terms. This is reflected by the computed Mulliken charges, which are equal for both rhenium atoms (0.57 each). The same is still true if the complete [(phen)Re(CO)$_3$]$^{+}$ fragments (0.47 each) are considered. Also, the DFT-optimized distances on both rhenium(I) tricarbonyl fragments are almost exactly equal, and close to the experimentally determined values. It is important to emphasize that the inclusion of the bromide counter-anion into the optimization does not change the situation, both metallic fragments remain still completely equivalents. It should be also noted that the inclusion of dispersion effects into the geometry optimization of **1**$^{+}$ leads to minor changes into the distances (see Table S2), suggesting that weak interactions (π-π and π-stacking) play a minor role in the structure of the cation. The optimized value for the bridging angle is 142.30°, larger than the value determined for each polymorph. Figure 3 shows an energy level diagram for the frontier Kohn-Sham orbitals determined for **1**$^{+}$. It clearly shows a metal centered HOMO and near HOMO levels, corresponding mainly to combinations of the so-called "t_{2g}"metallic orbitals whereas their vacant "e_g^*" counterparts are lying above the six $\pi^*_{(phen)}$ lowest unoccupied combinations. Figure S2 shows the complete set of frontier orbital calculated for **1**$^{+}$.

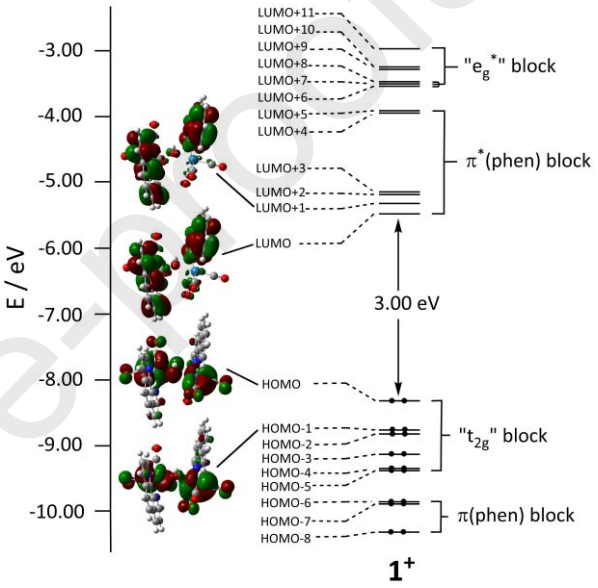

Figure 3. Kohn- Sham levels computed for **1**$^{+}$.

3.3 Spectroscopic Properties in Solution. Figure 4a shows the absorption spectra determined in solution for **1**$^{+}$Br^{-}. One may expect that; at least in principle and without considering coordination effects; after dissolving, each of the polymorphic forms described above should led to the same species in solution. The absorption spectra of **1**$^{+}$ in solution shows two broad and featureless absorption bands around 290 and 375 nm, depending on the solvent. In DCM, this last band becomes very flat, but 390 nm can be considered as the center. The unsensitivity of the absorption spectrum after emission measurements in non-coordinating and coordinating solvents rules out the breakdown of **1**$^{+}$ in the essayed conditions.

Also, the emission maxima do not show hypsochromic shift as observed for the monometallic related complex $[(phen)(H_2O)Re(CO)_3]^+(CF_3SO_3)^-$][48]**.** Based on their extinction coefficients and the comparison with related complexes, they can be assigned to $\pi_{(phen)} \rightarrow \pi^*_{(phen)}$ intraligand (IL) and $Re_{(d\pi)} \rightarrow \pi^*_{(phen)}$ metal to ligand charge transfer (MLCT) transitions, respectively.

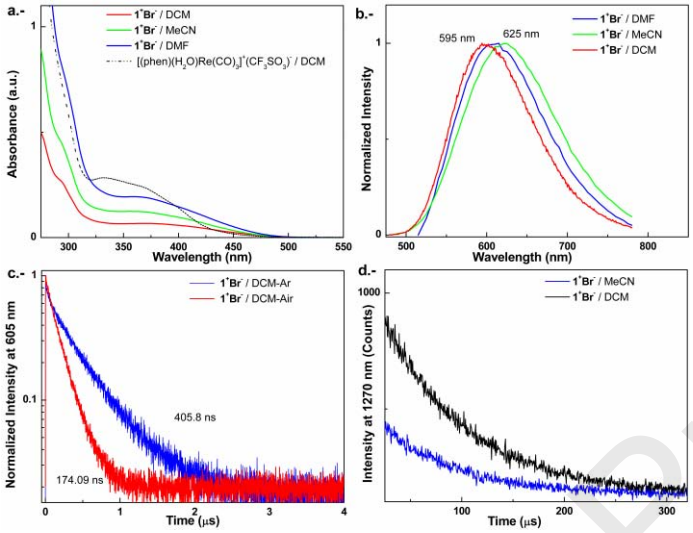

Figure 4. a.- Absorption spectra determined for $\mathbf{1}^+Br^-$ in DCM, DMF or MeCN solution. $[(phen)(H_2O)Re(CO)_3]^+(CF_3SO_3)^-$[48] included for comparison. **b.-** Emission spectra for $\mathbf{1}^+Br^-$ in DCM, DMF or MeCN solution. λ_{EX}: 405 nm. **c.-** Emission decay measured in argon(–) or air(–) equilibrated solution. **d.-** Emission decay of singlet oxygen generated by $\mathbf{1}^+$ in DCM and MeCN upon excitation at 405 nm.

For $\mathbf{2}^+$ the lowest energy band is also broad in DCM, being found to be around 375 nm [27], while for $[(phen)(H_2O)Re(CO)_3]^+(CF_3SO_3)^-$ it appears about 350 nm [48]. Figure 5 shows the TD-DFT computed spectra for $\mathbf{1}^+$ (fully and partly optimized) and $\mathbf{1}^+Br^-$, showing the main transitions. The Kohn-Sham levels implied into each transition are given in Table 2. These data are consistent with an MLCT character for the band observed around 375 nm for $\mathbf{1}^+Br^-$ in solution. The almost complete invariance of the TD-DFT computed spectra for $\mathbf{1}^+$ compared to $\mathbf{1}^+Br^-$ suggests that both, ionic pairing and bending angle would have a negligible effect on the light absorption by the compound.

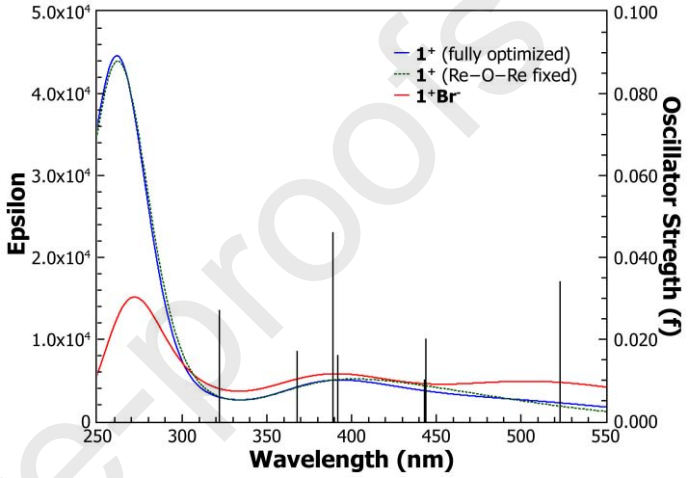

Figure 5. TDDFT computed spectra for $\mathbf{1}^+$ fully optimized, $\mathbf{1}^+$ optimized with te Re-O-Re bridging angle equal to 130.9 and $\mathbf{1}^+Br^-$. Oscillator strength (*f*) for the computed excitations for $\mathbf{1}^+$ are shown as bars.

Table 2. Summary of main energy, wavelength and oscillator strength (*f*) computed for observed transitions in the absorption spectra of $\mathbf{1}^+$, together with the orbitals implied.

N	E / eV	λ / nm	*f*	Major Contributions	Assignment
1	2.37	523	0.034	HOMO → LUMO (97%)	
5	2.79	444	0.020	HOMO-2 → LUMO+1 (23%)	
				HOMO-1 → LUMO (72%)	
6	2.80	443	0.010	HOMO-2 → LUMO (71%)	
				HOMO-1 → LUMO+1 (23%)	
13	3.16	392	0.016	HOMO-2 → LUMO+3 (34%)	$Re_{d\pi} \rightarrow \pi^*_{(phen)}$
				HOMO-1 → LUMO+2 (50%)	
14	3.19	389	0.046	HOMO-3 → LUMO+1 (54%)	
				HOMO-2 → LUMO+2 (13%)	
				HOMO-1 → LUMO+3 (24%)	
20	3.37	368	0.017	HOMO-5 → LUMO+1 (23%)	
				HOMO-3 → LUMO+2 (62%)	
27	3.86	322	0.027	HOMO-7 → LUMO+1 (16%)	
				HOMO-6 → LUMO (52%)	$\pi \rightarrow \pi^*_{(phen)}$
				HOMO → LUMO+4 (23%)	

The broad feature of the band associated with the transitions of lower energy is related to the substantial number of "t_{2g}" $\rightarrow$ $\pi^*_{(phen)}$ possible excitations, all within the same energy range.

Table 3 shows a summary of photophysical properties. Excitation of the bimetallic compound at 405 nm leads to a broad and unstructured emission band around 595 nm and 605 nm in dichloromethane and N,N-dimethylformamide solution, respectively (Figure 3b), while the emission is bathochromically shifted to 625 nm in acetonitrile.

As stated for similar compounds, the emission has mainly MLCT character [27, 45, 48]. A very rough approximate calculation of the emission wavelengths can be made by DFT-optimizing the geometry of the molecule in the first triplet configuration ($\mathbf{1}^+$ (S=1)) and then using this for computing the vertical excitations by TD-DFT [49]. Table S5 shows the main results of this procedure, setting the HOMO $\rightarrow$ LUMO and HOMO $\rightarrow$ LUMO+1 excitations to be at 622 and 578 nm, respectively, which is consistent with what is observed experimentally.

The rather invariance in the emission wavelength for $\mathbf{1}^+$ going from DCM to DMF has been attributed to the ability of the carbonyl stretching modes to act as a vibrational acceptor of the excited-state energy [45, 50], making the emission unsensitive to solvent polarity. The bathochromic shift to 625 nm observed in acetonitrile has been described previously as arising from hydrogen bonding between the aquo fragment in $[(phen)(H_2O)Re(CO)_3]^+(CF_3SO_3)^-$ with N,N-dimethylformamide solvent molecules [48]. The existence of the effect for acetonitrile instead of N,N-dimethylformamide would be attributed to the steric limitation imposed by the hydroxyl bonding between metallic fragments compared to $[(phen)(H_2O)Re(CO)_3]^+$. The center of the emission band measured in dichloromethane for 2^+ is 608 nm (λ_{ex} = 375 nm) [27]. As shown in Figure 3c, the emission of $\mathbf{1}^+$ in argon-equilibrated dichloromethane solution at 605 nm follow a mono-exponential decay with a lifetime equal to 405.8 ns, which is considerably shortened to 174.09 ns in air-equilibrated DCM solution. This strongly suggests a considerably triplet character for the emitting state. Confirming this, Figure 3d shows the direct phosphorescent emission detection at 1270 nm of singlet oxygen generated by $\mathbf{1}^+$ in dichlorometane and acetonitrile solutions. In contrast, the emission of $\mathbf{2}^+$ in dichlorometane solution decays following a bi-exponential law, with a major component (80% in amplitude) of 136 ns and a minor (20%) of 7 ns.

3.4 Spectroscopic Properties in Solid. In order to contrast the photophysical properties in solution, were the geometry of 1^+ would relax, and consequently to test the influence of the Re–O–Re bridging angle on them, we have performed solid state characterization of the polymorphic mixture of $\mathbf{1}^+Br^-$.

Figure 6a shows the transmittance of the solid compound as a function of the wavelength. It shows the solid has very broad absorption band with a maximum around 460 nm (390 nm in DCM).

Table 3. Summary of the main photophysical properties of $\mathbf{1}^+$.

Solvent	λ_{abs}/nm	$\lambda_{em,air}$/nm	$\tau_{em,air}$/ns[a]	$\Phi_{em,\ air}$	$\lambda_{em,\ Ar}$ /nm	$\Phi_{em,\ Ar}$	$\tau_{em,\ Ar}$/ns[a]	Φ_{Δ}[b]
DCM	295; 390	595	174	0.032	605	0.067	406	0.21
DMF	295; 380	605	102	0.016	605	0.038	283	0.40
MeCN	295; 375	625	71	0.010	625	0.033	311	0.47

* Errors were lower than 10%. λ_{ex} = 405 nm. [a] amplitudes are reported in parentheses. [b] Values for singlet oxygen generation.

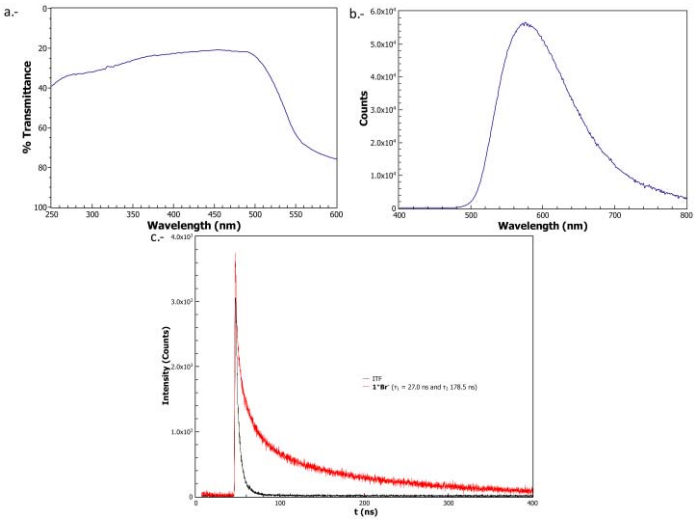

Figure 6. a.- Transmittance spectra determined for the solid polymorphic mixture of $\mathbf{1}^{+}Br^{-}\cdot x(CHCl_3)$. **b.-** Emission spectrum for the solid polymorphic mix of $\mathbf{1}^{+}Br^{-}\cdot x(CHCl_3)$. λ_{ex}: 320 nm. **c.-** Emission decay for the solid polymorphic mixture of $\mathbf{1}^{+}Br^{-}\cdot x(CHCl_3)$.

Excitation of the solid compound at 320 nm leads to a broad (but symmetric) emission band between approximately 500 and 700 nm, with a maximum at 575 nm. This last value matches quite well with the 595 nm observed for the emission maximum in DCM solution. In the same way, the emission decay follows in the solid state a bi-exponential law. The lifetimes observed for the solid-state emission, 27.0 ns and 178.5 ns, suggest that we still have the same de-excitation process as the one observed in the air (174.09 ns) but also a faster de-excitation process maybe due to the closer distances between the species found in the solid state compared to those in solution.

4. Conclusions

Results show that dimers of the type $[(CO)_3$(N,N-diimine)Re(μ-X)Re(N,N-diimine)$(CO)_3]^{+}$ may be formed as by-products during the synthesis of monometallic rhenium(I) tricarbonyls in a general way, as a result of the presence of adventitious water or some other molecule acting as a Lewis base. X-ray diffraction structural results for the three polymorphic forms of $[(CO)_3(phen)Re(\mu\text{-}OH)Re(phen)(CO)_3]^{+}$ ($\mathbf{1}^{+}$) cation shows that the Re^{I}-O(H)-Re^{I} bridging angle would vary significantly depending on the packing structure. This effect offers a unique possibility opportunity to analyze the effect of the geometry on the photo-physical properties of a molecule. The comparison of the photophysical properties in solution, where a relaxed geometry for $\mathbf{1}^{+}$ exists, with those obtained in the solid state, where the geometry of $\mathbf{1}^{+}$ is rigid and subjected to packing effects, suggest the Re^{I}-O(H)-Re^{I} bridging does not affect them significantly. Actually we have work in progress focused on the synthesis of new examples of the $[(CO)_3(N,N)Re(\mu\text{-}X)Re(N,N)(CO)_3]^{+}$ cation, for a full understanding of the effect of the size and nature of X on its photophysical properties.

Appendix A. Supplementary data.

Crystal data in the Crystallographic Information File (cif) format have been deposited in CSD under codes CCDC1896852 ($\mathbf{1}^{+}\mathbf{Br}^{-}\cdot CHCl_3$, triclinic), CCDC1896850 ($\mathbf{1}^{+}\mathbf{Br}^{-}\cdot CHCl_3$, orthorhombic) and CCDC1896848 ($\mathbf{1}^{+}\mathbf{Br}^{-}\cdot 2(CHCl_3)$ (triclinic)). These data can be obtained free of charge via http://www.ccdc.cam.ac.uk/conts/retrieving.html , or from the Cambridge Crystallographic Data Centre, 12 Union Road, Cambridge CB2 1EZ, UK; fax: (+44) 1223-336-033; or e-mail: deposit@ccdc.cam.ac.uk. Optimized coordinates for $\mathbf{1}^{+}$, $\mathbf{1}^{+}\mathbf{Br}^{-}$, $\mathbf{1}^{+}$ (Dispersion correction) and $\mathbf{1}^{+}$ (S=1). Supplementary data associated with this article can be found, in the online version, at http://dx.doi.org/xxxxx

Acknowledgements

The authors acknowledge partial financial support from Fondecyt 3170100, 1160546, 1160749, PIA Conicyt Anillo ACT 1404, and

Financiamiento Basal para Centros Científicos y Tecnológicos de Excelencia FB0807. This research has been performed as part of the Chilean–French International Associated Laboratory for ‘‘Multifunctional Molecules and Materials’’ (LIA M3 - CNRS No. 1207).

References

[1] A. Kumar, S.-S. Sun, A.J. Lees, Photophysics and Photochemistry of Organometallic Rhenium Diimine Complexes, in: A.J. Lees (Ed.) Photophysics of Organometallics, Springer, Berlin, Heidelberg, 2010, pp. 37-71.

[2] A. Vlček, Ultrafast Excited-State Processes in Re(I) Carbonyl-Diimine Complexes: From Excitation to Photochemistry, in: A.J. Lees (Ed.) Photophysics of Organometallics, Springer, Berlin, Heidelberg, 2010, pp. 115-158.

[3] D.J. Stufkens, A. Vlček, Ligand-dependent excited state behaviour of Re(I) and Ru(II) carbonyl–diimine complexes, Coordination Chemistry Reviews, 177 (1998) 127-179.

[4] L.M. Kiefer, J.T. King, K.J. Kubarych, Dynamics of rhenium photocatalysts revealed through ultrafast multidimensional spectroscopy, Acc Chem Res, 48 (2015) 1123-1130.

[5] S. Sato, T. Arai, T. Morikawa, Toward Solar-Driven Photocatalytic CO_2 Reduction Using Water as an Electron Donor, Inorg Chem, 54 (2015) 5105-5113.

[6] T.A. Oriskovich, P.S. White, H.H. Thorp, Luminescent Labels for Purine Nucleobases - Electronic-Properties of Guanine Bound to Rhenium(I), Inorganic Chemistry, 34 (1995) 1629-1631.

[7] K.K. Lo, M.W. Louie, K.S. Sze, J.S. Lau, Rhenium(I) polypyridine biotin isothiocyanate complexes as the first luminescent biotinylation reagents: synthesis, photophysical properties, biological labeling, cytotoxicity, and imaging studies, Inorg Chem, 47 (2008) 602-611.

[8] L.L.S. Man, C.W. Kin, Photosensitizing Properties of Some Rhenium(I) Tricarbonyl Diimine Complexes, ChemPhysChem, 2 (2001) 252-256.

[9] K.-C. Chang, S.-S. Sun, M.O. Odago, A.J. Lees, Anion recognition and sensing by transition-metal complexes with polarized NH recognition motifs, Coordination Chemistry Reviews, 284 (2015) 111-123.

[10] K.C. Chang, S.S. Sun, A.J. Lees, Anion sensing by rhenium(I) carbonyls with polarized N-H recognition motifs, Inorganica Chimica Acta, 389 (2012) 16-28.

[11] M. Salmain, M. Gunn, A. Gorfti, S. Top, G. Jaouen, Labeling of proteins by organometallic complexes of rhenium. (I). Synthesis and biological activity of the conjugates, Bioconjugate chemistry, 4 (1993) 425-433.

[12] G. Santoro, T. Zlateva, A. Ruggi, L. Quaroni, F. Zobi, Synthesis, characterization and cellular location of cytotoxic constitutional organometallic isomers of rhenium delivered on a cyanocobalmin scaffold, Dalton Trans, 44 (2015) 6999-7008.

[13] K. Wahler, A. Ludewig, P. Szabo, K. Harms, E. Meggers, Rhenium Complexes with Red-Light-Induced Anticancer Activity, Eur. J. Inorg. Chem., 2014 (2014) 807-811.

[14] D.L. Ma, C.M. Che, F.M. Siu, M. Yang, K.Y. Wong, DNA binding and cytotoxicity of ruthenium(II) and rhenium(I) complexes of 2-amino-4-phenylamino-6-(2-pyridyl)-1,3,5-triazine, Inorg Chem, 46 (2007) 740-749.

[15] M.W. Louie, A.W.T. Choi, H.W. Liu, B.T.N. Chan, K.K.W. Lo, Synthesis, Emission Characteristics, Cellular Studies, and Bioconjugation Properties of Luminescent Rhenium(I) Polypyridine Complexes with a Fluorous Pendant, Organometallics, 31 (2012) 5844-5855.

[16] C.D. Windle, M.V. Campian, A.K. Duhme-Klair, E.A. Gibson, R.N. Perutz, J. Schneider, CO_2 photoreduction with long-wavelength light: dyads and monomers of zinc porphyrin and rhenium bipyridine, Chem Commun (Camb), 48 (2012) 8189-8191.

[17] C.D. Windle, E. Pastor, A. Reynal, A.C. Whitwood, Y. Vaynzof, J.R. Durrant, R.N. Perutz, E. Reisner, Improving the photocatalytic reduction of CO_2 to CO through immobilisation of a molecular Re catalyst on TiO_2, Chemistry, 21 (2015) 3746-3754.

[18] T.W. Schneider, A.M. Angeles-Boza, Competitive ^{13}C and ^{18}O kinetic isotope effects on CO_2 reduction catalyzed by Re(bpy)$(CO)_3$Cl, Dalton Trans, 44 (2015) 8784-8787.
[19] F. Franco, C. Cometto, C. Garino, C. Minero, F. Sordello, C. Nervi, R. Gobetto, Photo- and Electrocatalytic Reduction of CO_2 by [Re$(CO)_3${α,α'-diimine-(4-piperidinyl-1,8-naphthalimide)}Cl] Complexes, European Journal of Inorganic Chemistry, (2015) 296-304.
[20] G. Sahara, O. Ishitani, Efficient Photocatalysts for CO_2 Reduction, Inorg Chem, 54 (2015) 5096-5104.
[21] J. Agarwal, E. Fujita, H.F. Schaefer, 3rd, J.T. Muckerman, Mechanisms for CO production from CO2 using reduced rhenium tricarbonyl catalysts, J Am Chem Soc, 134 (2012) 5180-5186.
[22] T. Morimoto, T. Nakajima, S. Sawa, R. Nakanishi, D. Imori, O. Ishitani, CO_2 capture by a rhenium(I) complex with the aid of triethanolamine, J Am Chem Soc, 135 (2013) 16825-16828.
[23] J. Shakeri, H. Hadadzadeh, H. Tavakol, Photocatalytic reduction of CO_2 to CO by a dinuclear carbonyl polypyridyl rhenium(I) complex, Polyhedron, 78 (2014) 112-122.
[24] A.J. Lees, Luminescence Properties of Organometallic Complexes, Chem Rev, 87 (1987) 711-743.
[25] L. Sacksteder, A.P. Zipp, E.A. Brown, J. Streich, J.N. Demas, B.A. Degraff, Luminescence Studies of Pyridine Alpha-Diimine Rhenium(I) Tricarbonyl Complexes, Inorganic Chemistry, 29 (1990) 4335-4340.
[26] J.L. Smithback, J.B. Helms, E. Schutte, S.M. Woessner, B.P. Sullivan, Preparative routes to luminescent mixed-ligand rhenium(I) dicarbonyl complexes, Inorg Chem, 45 (2006) 2163-2174.
[27] H. Gallardo, M. Cepeda-Plaza, S. Nonell, G. Günther, E. Chamorro, N. Pizarro, A. Vega, Structural and photophysical properties of [(CO)3(phen)Re(μ-Br)Re(phen)(CO)3]+[(CO)3Re(μ-Br)3Re(CO)3]−: Where does its luminescence come from?, Polyhedron, 97 (2015) 227-233.
[28] K. Ruth, T. Morawitz, H.-W. Lerner, M. Bolte, [mu]-Hydroxido-bis[(2,2'-bipyridine)tricarbonylrhenium(I)] perrhenate, Acta Crystallographica Section E, 64 (2008) m496.
[29] L. Cuesta, D.C. Gerbino, E. Hevia, D. Morales, M.E. Navarro Clemente, J. Pérez, L. Riera, V. Riera, D. Miguel, I. del Río, S. García-Granda, Reactivity of Molybdenum and Rhenium Hydroxo-Carbonyl Complexes toward Organic Electrophiles, Chemistry – A European Journal, 10 (2004) 1765-1777.
[30] P.J. Heard, P. Sroisuwan, D.A. Tocher, Synthesis and reactivity of N,N,N',N'-tetramethyldiaminomethane complexes of tricarbonylrhenium(I). X-ray molecular structures of [ReBr(CO)3(TMDM)] and [{Re(bipy)(CO)3}2(μ-OH)][SbF6], Polyhedron, 22 (2003) 1321-1327.
[31] D.H. Gibson, M.S. Mashuta, X. Yin, [mu]-Hydroxo-bis[(4,4'-dimethyl-2,2'-bipyridine)tricarbonylrhenium(I)] perrhenate acetone hemisolvate, Acta Crystallographica Section E, 59 (2003) m911-m913.
[32] Bruker, APEX2, SAINT and SADABS, in: M. Bruker AXS Inc., Wisconsin, USA. (Ed.), 2012.
[33] G. Sheldrick, Crystal structure refinement with SHELXL, Acta Crystallographica Section C, 71 (2015) 3-8.
[34] G.M. Sheldrick, A short history of SHELX, Acta Crystallogr., A64 (2008) 112-122.
[35] H. Rietveld, A profile refinement method for nuclear and magnetic structures, Journal of Applied Crystallography, 2 (1969) 65-71.
[36] Diffrac.TOPAS suite General profile and structure analysis software for powder diffraction data, in, Diffrac.TOPAS suite General profile and structure analysis software for powder diffraction data: Bruker AXS, Karlsruhe, Germany, 2009.
[37] G.A. Crosby, J.N. Demas, Measurement of photoluminescence quantum yields. Review, The Journal of Physical Chemistry, 75 (1971) 991-1024.
[38] K. Suzuki, A. Kobayashi, S. Kaneko, K. Takehira, T. Yoshihara, H. Ishida, Y. Shiina, S. Oishi, S. Tobita, Reevaluation of absolute luminescence quantum yields of standard solutions using a spectrometer

with an integrating sphere and a back-thinned CCD detector, Physical Chemistry Chemical Physics, 11 (2009) 9850-9860.
[39] R. Schmidt, C. Tanielian, R. Dunsbach, C. Wolff, Phenalenone, a universal reference compound for the determination of quantum yields of singlet oxygen $O_2(^1\Delta_g)$ sensitization, Journal of Photochemistry and Photobiology A: Chemistry, 79 (1994) 11-17.
[40] A.A. Abdel-Shafi, D.R. Worrall, A.Y. Ershov, Photosensitized generation of singlet oxygen from ruthenium(ii) and osmium(ii) bipyridyl complexes, Dalton Transactions, (2004) 30-36.
[41] M.J.T. Frisch, G. W.; Schlegel, H. B.; Scuseria, G. E.; Robb, M. A.; Cheeseman, J. R.; Scalmani, G.; Barone, V.; Mennucci, B.; Petersson, G. A.; Nakatsuji, H.; Caricato et al., Gaussian 09, in, Gaussian, Inc., Wallingford CT, 2009.
[42] S. Grimme, J. Antony, S. Ehrlich, H. Krieg, A consistent and accurate ab initio parametrization of density functional dispersion correction (DFT-D) for the 94 elements H-Pu, The Journal of Chemical Physics, 132 (2010) 154104.
[43] A.J. Lees, The Luminescence Rigidochromic Effect Exhibited by Organometallic Complexes: Rationale and Applications, Comments on Inorganic Chemistry, 17 (1995) 319-346.
[44] W. Humphrey, A. Dalke, K. Schulten, VMD: visual molecular dynamics, J. Mol. Graphics, 14 (1996) 33-38, 27-38.
[45] R.M. Spada, M. Cepeda-Plaza, M.L. Gómez, G. Günther, P. Jaque, N. Pizarro, R.E. Palacios, A. Vega, Clean Singlet Oxygen Production by a Re^{I} Complex Embedded in a Flexible Self-Standing Polymeric Silsesquioxane Film, The Journal of Physical Chemistry C, 119 (2015) 10148-10159.
[46] Angel A. Martí, G. Mezei, L. Maldonado, G. Paralitici, Raphael G. Raptis, Jorge L. Colón, Structural and Photophysical Characterisation of fac-[Tricarbonyl(chloro)(5,6-epoxy-1,10-phenanthroline)rhenium(I)], European Journal of Inorganic Chemistry, 2005 (2005) 118-124.
[47] I. Chakraborty, J. Jimenez, W.M.C. Sameera, M. Kato, P.K. Mascharak, Luminescent Re(I) Carbonyl Complexes as Trackable PhotoCORMs for CO delivery to Cellular Targets, Inorganic Chemistry, 56 (2017) 2863-2873.
[48] P. Mella, K. Cabezas, C. Cerda, M. Cepeda-Plaza, G. Günther, N. Pizarro, A. Vega, Solvent, coordination and hydrogen-bond effects on the chromic luminescence of the cationic complex $[(phen)(H_2O)Re(CO)_3]^+$, New Journal of Chemistry, 40 (2016) 6451-6459.
[49] C. Adamo, D. Jacquemin, The calculations of excited-state properties with Time-Dependent Density Functional Theory, Chemical Society Reviews, 42 (2013) 845-856.
[50] J.V. Caspar, T.J. Meyer, Application of the energy gap law to nonradiative, excited-state decay, The Journal of Physical Chemistry, 87 (1983) 952-957.